NANOSCALE AND MICROSCALE THERMOPHYSICAL ENGINEERING
2017, VOL. 21, NO. 1, 8–25
http://dx.doi.org/10.1080/15567265.2016.1263696

Taylor & Francis
Taylor & Francis Group

On Investigating the Thermomechanical Properties of Cross-linked Epoxy Via Molecular Dynamics Analysis

Yao Fu[a], John G. Michopoulos[b], and Jeong-Hoon Song[c]

[a]Department of Aerospace Engineering and Engineering Mechanics, University of Cincinnati, Cincinnati, Ohio, USA; [b]Computational Multiphysics Systems Laboratory, Naval Research Laboratory, Washington, D.C., USA; [c]Department of Civil, Environmental, and Architectural Engineering, University of Colorado, Boulder, Colorado, USA

ABSTRACT

In this work, we demonstrate the feasibility of a computational approach based on first principles for estimating various thermomechanical quantities of a cross-linked epoxy resin. In particular, this work is focused on determining estimated values of the variation in glass transition temperature, coefficient of thermal expansion, volume shrinkage due to curing, Young's modulus, Poisson's ratio, yield strength, and viscosity as a function of temperature and degree of curing via molecular dynamics simulations. In most cases it has been demonstrated that the values predicted by the proposed approach are in good agreement with the respective experimentally measured values. In addition, the validity of the proposed models describing the dependence of the thermomechanical quantities on temperature and curing degree is examined. Throughout this study, we demonstrate that the molecular dynamics–based computational predictive framework can serve as an excellent infrastructure that can enable numerical prediction of materials properties and thereby can reduce the costs of associated with physical experimentation. In addition, we demonstrate that insightful information can be generated at the molecular and microscopic scales that is not easily extractable from experiments.

ARTICLE HISTORY
Received 17 July 2016
Accepted 18 November 2016

KEYWORDS
Full atomistic molecular dynamics; cross-linking; thermomechanical properties; epoxy resin

Introduction

Polymer matrix composites are widely used in many areas of application, including aviation, marine, and automotive industries for manufacturing various parts and components [1]. Given the high volume and large composite parts production, there is an immediate need for the optimization of a manufacturing process to obtain the desired performance of a product. The need for functional performance specification and data-driven tailoring of the manufacturing process of composites for optimizing their performance has already been introduced elsewhere [2]. The combination of the intrinsic material anisotropy and heterogeneity due to the fiber reinforcement and the angle-ply laminates combined with manufacturing control parameters such as temperature and vacuum pressure applied during an autoclave manufacturing process affect the manifestation of various types of defects such as voids, ply waviness, delamination, fiber wrinkling, resin starvation/rich areas, and warpage [3–6], which in turn affect some of the material properties. However, predicting the presence and characteristics of these manufacturing defects involves consideration of various factors. One of these factors is the fact that the basic formulation of preimpregnated fiber-reinforced composites, which has been widely used for fabricating high-performance composite components, often includes curable epoxy resin–hardener system and fibers.

CONTACT Yao Fu yao.fu@colorado.edu Department of Aerospace Engineering and Engineering Mechanics, University of Cincinnati, 2850 Campus Way, Room 745 Baldwin Hall ML 0070,Cincinnati, OH 45221, USA; Jeong-Hoon Song jhsong@colorado.edu Department of Civil, Environmental, and Architectural Engineering, University of Colorado, 1111 Engineering drive, 428 UCB, Boulder CO 80309, USA.

Color versions of one or more of the figures in the article can be found online at www.tandfonline.com/umte.

The thermomechanical properties of these epoxy resin–hardener systems can vary significantly with pressure and temperature due to the cross-linking process [7–12]. In addition, without an accurate prediction of the pressure- and temperature-dependent thermomechanical properties of the epoxy resin system during the curing process, it is difficult to predict the evolution of the manufacturing defects.

Computational approaches provide an excellent route to characterize materials properties by reducing the cost of exhaustive hit-and-miss experimentation and by providing insightful information at the molecular and microscopic scales not easily extracted from experiments [13, 14]. Recently, several theroretical studies based on the understanding of the atomistic behaviors of polymeric structures have contributed to the modeling of thermoset polymers such as an epoxy resin system that builds a cross-linked network between the polymer chains during the curing (cross-linking) process. Most widely used techniques include coarsed-grained (CG) molecular dynamics [15, 16] simulation and Monte Carlo simulation [17, 18]. Though CG models can predict accelerated dynamics and reach time- and length scales unachieveable by full atomistic simulation, the simplied models often cannot predict all materials properties with one set of CG parameters. In most situations, the virtually characterized physical properties need to be verifed against full atomisitc simulation before application.

Due to the importance of cross-linked polymers in various applications [13, 14, 19–21], there have been increasing studies on polymer networks in addition to linear homopolymers or copolymers [22–27]. Wu and Xu [25] investigated a computational method for the construction of a polymer network based on diglycidyl ether bisphenol A (DGEBA) and isophorone diamine (IPD). They successfully generated the network with conversion up to 93.7% and estimated the elastic constants and density from the equilibrated structure via molecular dynamics (MD) simulations. The interfacial interactions between carbon nanotubes and cured epoxy resin (EPON-862) in terms of stress transfer have been studied by Gou et al. [28] using Accelyrs. Insightful information regarding the interfacial interactions and materials properties has been provided in these studies. Fan and Yuen [29] evaluated the materials properties of an EPON-862/TETA thermoset system. Wu and Xu [30] performed cross-linking simulations for epoxy resins, which were further used to study the diffusion of water in these cross-linked networks. Relative limited work has been done to investigate the cross-linking-dependent thermomechanical properties by molecular simulations although the degree of cross-linking is well known to affect the bulk effective properties. Komarov et al. [31] proposed a four-step reverse mapping procedure using the Monte Carlo/MD hybrid scheme to study the physical behavior of highly dense network as a function of cure conversion. Varshney et al. [24] proposed a multistep relaxation procedure for relaxing the molecular topology during cross-linking and characterized the materials properties of an epoxy-based thermoset system (EPON-862/DETDA) at various cure conversions. Li and Strachan [23] studied an EPON-862/DETDA epoxy system and predicted a significant increase in glass transition temperature, stiffness, and yield stress with cure conversion.

In the present study, we build a commercially widely used epoxy resin system of different cross-linking degrees via MD simulation and estimate various thermomechanical properties including the glass transition temperature, thermal expansion coefficient, curing-induced shrinkage, elastic modulus, yield stress, and viscosity; the chemical composition of the epoxy resin system considered herein includes DGEBA and IPD, where DGEBA is also known as EPON 828 and can be cross-linked in the presence of amine hardeners to yield one of the most frequently used epoxy polymers in structural composites and coatings. Because of the wide applicability of this epoxy resin system, our simulation results have also been compared with the readily available experimental data and fitted with empirical models established for describing the temperature- and curing degree–dependent thermomechanical properties.

Modeling and simulation details

Force field

The initial molecular dynamics model of the un-cross-linked epoxy resin system is shown in Figures 1a and 1b. The molecular models are built in Accelyrs/Biovia Materials Studio [32] with a

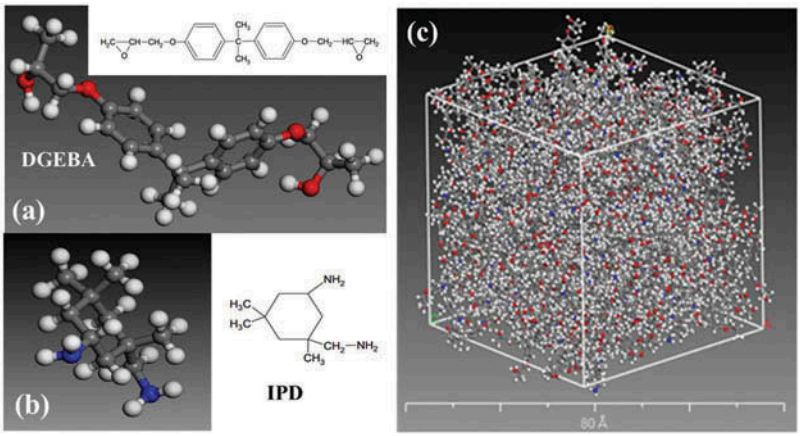

Figure 1. Structure of (a) resin, (b) cross-linker molecules, and (c) and resin system built in the Materials Studio package.

stoichiometric mixture of 200 DGEBA+100 IPD, using the amorphous cell module at an initial density of 1.13 g/cm^3 (Figure 1c) [33]. Partial charges of atoms were assigned based on the polymer consistent force field (PCFF), and periodic boundary conditions are imposed on the cubic unit cell in order to eliminate surface effects.

The PCFF force field adopted in the present study [34, 35] is developed based on the consistent-valence force field (CFF) for biologically interesting molecules. Like the CFF93 force field [35], PCFF is an ab initio force field where most parameters were derived based on the ab initio data using a least-squares-fit technique developed by Maple et al. [36]. Many of the nonbonded parameters of PCFF are taken from the CFF91 force field [37], including atomic partial charges and Lennard-Jones 9-6 (LJ-9-6) parameters. The total energy is divided into terms that fall in three major categories: (a) contributions from each of the internal valence coordinates of bond (b), angle (θ), torsion angle (ϕ), and out-of-plane angle (χ); (b) cross-coupling terms including the combinations of two or three internal coordinates; and (c) nonbonded interactions. The valence energies consist of terms from distortions of bond lengths E^b, bond angles E^θ, out-of-plane bending angles E^χ, and torsion angles E^ϕ. Both bond and angle terms contain up to quartic terms to characterize anharmonic features. The torsion function is represented by a symmetric Fourier expansion. The out-of-plane function is a simple harmonic function. Several cross-coupling terms are used in this force field: E^{bb}, $E^{b\theta}$, $E^{\theta\theta'}$, $E^{b\phi}$, $E^{\theta\phi}$, and $E^{\theta\theta'\phi}$ represent bond–bond, bond–angle, angle–angle, bond–torsion, angle–torsion, and angle–angle–torsion coupling terms, respectively. The nonbonded energies include intramolecular nonbonded interactions, which are interactions between any pair of atoms that belong to the same molecule but are separated by at least two intervening atoms, and intermolecular nonbonded interactions, which are the interactions between any pair of atoms that belong to different molecules. The nonbonded energies are subsequently divided into van der Waals interactions E^{vdw} and electrostatic interactions E^{elec}. A 9-6 Lennard-Jones function is used to represent the van der Waals forces characterized by the atom size r^* and interaction strength ε, and the electrostatic interaction is written in the form of a standard Coulombic interaction with partial atomic charges, which are written as a sum of bond increments δ_{ij}, defined as a charge displacement from atom i to atom j as $Q_i = \sum_j \delta_{ij}$.

The functional forms of this consistent PCFF force field are given in terms of the valence potential energy contributions as

$$E_{total} = \sum_b E^b + \sum_\theta E^\theta + \sum_\phi E^\phi + \sum_\chi E^\chi + \sum_b \sum_{b'} E^{bb'} + \sum_b \sum_\theta E^{b\theta} + \sum_b \sum_\phi E^{b\phi} + \sum_\theta \sum_{\theta'} E^{\theta\theta'},$$
$$+ \sum_\theta \sum_\phi E^{\theta\phi} + \sum_\theta \sum_{\theta'} \sum_\phi E^{\theta\theta'\phi} + \sum_{i>j} E^{vdw} + \sum_{i>j} E^{elec}$$

where

$$E^{b} = \sum_{n=2}^{4} k^{bn}(b - b_0)^n \tag{1b}$$

$$E^{\theta} = \sum_{n=2}^{4} k^{\theta n}(\theta - \theta_0)^n \tag{1c}$$

$$E^{\phi} = \sum_{n=1}^{3} k^{\phi n}(1 - \cos n\phi) \tag{1d}$$

$$E^{\chi} = k^{\chi 0}\left(\chi - \chi_0\right)^2 \tag{1e}$$

$$E^{bb'} = k^{bb'}(b - b_0)(b' - b_0^{'}) \tag{1f}$$

$$E^{b\theta} = k^{b\theta}(b - b_0)(\theta - \theta_0) \tag{1g}$$

$$E^{b\phi} = (b - b_0)\sum_{n=1}^{3} k^{b\phi n}\cos n\phi \tag{1h}$$

$$E^{\theta\theta'} = k^{\theta\theta'}(\theta - \theta_0)\left(\theta' - \theta_0'\right) \tag{1i}$$

$$E^{\theta\phi} = (\theta - \theta_0)\sum_{n=1}^{3} k^{\theta\phi n}\cos n\phi \tag{1j}$$

$$E^{\theta\theta\phi} = k^{\theta\theta\phi}(\theta - \theta_0)\left(\theta' - \theta_0'\right)\cos\phi \tag{1k}$$

and

$$E^{vdw} = \varepsilon\left[2\left(r^*/r_{ij}\right)^9 - 3\left(r^*/r_{ij}\right)^6\right] \tag{1l}$$

$$E^{elec} = Q_i Q_j / r_{ij}, \tag{1m}$$

where the unstrained values of internal coordinates are denoted by the subscript 0, r^{ij} is the interatomic distance between atom i and j, and the parameters k^{ij} are the force constants for the corresponding intramolecular deformation [34, 35, 38, 39].

Cross-linking simulation

Cross-linking process simulation was conducted by creating bonds between reactive sites in close proximity. Two principal reactions taking place in this epoxy system are considered here as illustrated in Figure 2, where epoxy groups react with primary amine hydrogens to form secondary amines, which can further react with epoxy groups. The cross-linking procedure is similar to that proposed by Wu and Xu [25] and illustrated in Figure 3:

(1) Active hydrogens on end functional groups are firstly removed from the initially built epoxy system and reactive sites for nitrogen or carbon are left.
(2) Energy minimization is performed followed by 1,000 steps of MD simulation to relax the system, which was then analyzed in order to identify the reactive sites in close proximity. One of the reactive sites' carbons in DGEBAs is first chosen and then a search of nearby reactive sites' nitrogens in IPDs is conducted. The bonds will be created between a pair of sites with the smallest distance among possible pairs and the reaction cutoff distance ranges from 4 to 10 Å.
(3) The system is relaxed by another circle of molecular mechanics (MM) and MD to remove any unfavorable interactions due to the formation of new bonds. In addition, possible ring catenation or spearing is identified and removed from the system.

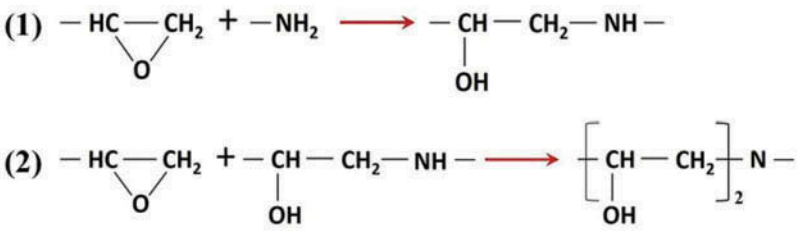

Figure 2. Two principal reactions involved in the curing of a diamine with a diepoxide.

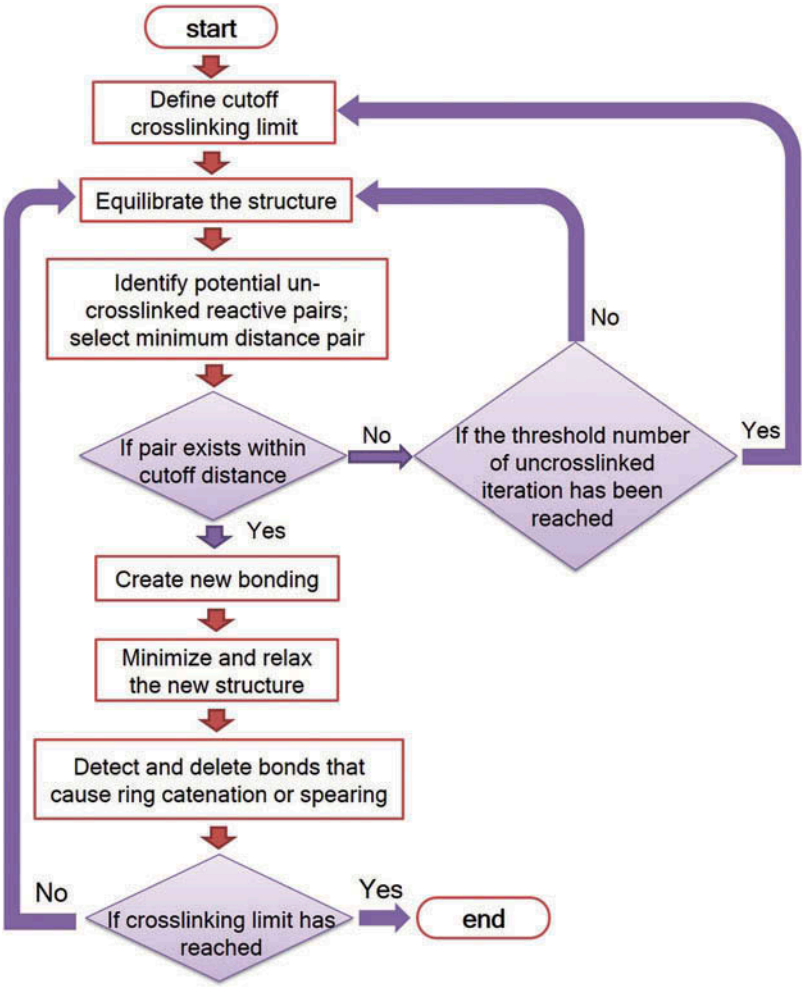

Figure 3. Flowchart that demonstrates the cross-linking algorithm.

(4) Steps 2 and 3 are repeated until the conversion reaches the desired cross-linking degree. To accelerate the conversation rate, two approaches are often adopted; that is, extending the reaction cutoff distance to a larger level and raising the temperature to a higher value. Finally, the nonhydrogen atoms in the cell system are saturated with hydrogen atoms for the subsequent simulations. These steps are performed alternatively using the large-scale atomic/molecular massively parallel simulator (LAMMPS) [40] and Materials Studio

package, where reactive sites identification and bond creation are conducted in LAMMPS and ring catenation or spearing check as well as hydrogen saturation are conducted in Materials Studio. After subsequent equilibration at high temperature, as shown in Figure 4, the created bond length distribution has only been changed slightly at various cross-linking degrees.

Annealing and uniaxial deformation simulation

To study the temperature dependence of various thermodynamic quantities, the cross-linked epoxies are further equilibrated under an isothermal–isobaric ensemble at high temperature (500 K) before the cooling simulation starts. Then a cooling simulation is performed where the different-level cross-linked systems are slowly cooled down at the rate of 5E10 K s^{-1} from 500 to 25 K under the atmospheric pressure, which is controlled by a Nose-Hoover thermostat and barostat [41, 42]. Tensile and compressive loading is conducted at the constant strain rate of 1E9 and 1E10 s^{-1} at varying temperatures across the glass transition regime by deforming the simulation box in the x direction, and the lateral dimensions (in y and z directions) are controlled by the barostat to keep the pressure at constant 1 bar. The loading continues until a true strain of 100% is reached. A time step size of 1 fs is employed throughout the MD simulation. All MD simulations are performed using LAMMPS. The snapshots for visualization are generated using a visual molecular dynamics graphics package. Time averaging of the density at each temperature in the annealing test and the stress tensor in the uniaxial deformation test is performed over 500 time instances. In this section and the subsequent Couette flow test, one sample is employed at each temperature, but the simulations are conducted multiples times with different initial states (atomic velocities and positions) to ensure reliability of the results.

Couette flow simulation

The important rheological quantity of the epoxy fluid, such as shear viscosity η, is studied through homogenous shear nonequilibrium molecular dynamics simulation using the SLLOD algorithm [43, 44] (Figure 5). A detailed description of the Lees-Edward model and SLLOD algorithm can be found in our

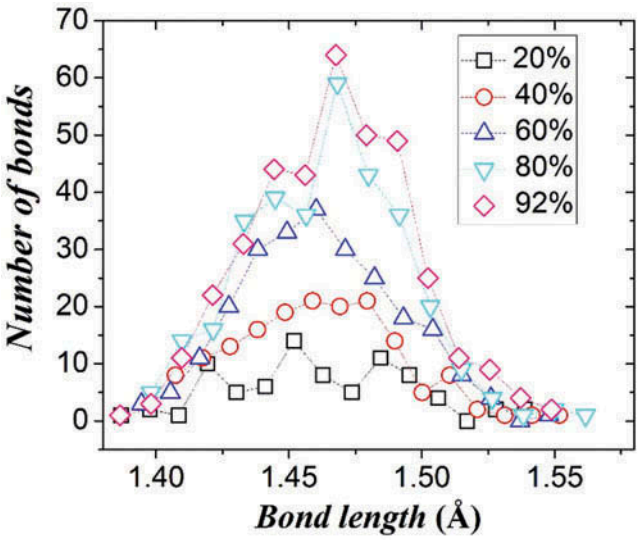

Figure 4. Created bond length distribution at different cross-linking degrees.

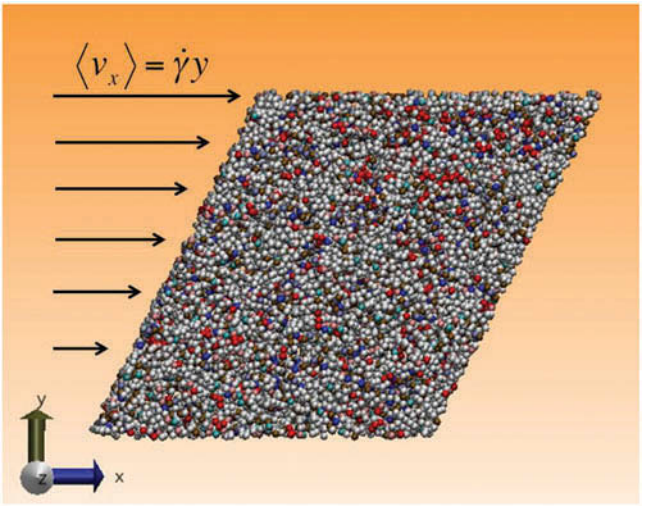

Figure 5. Schematic of the Couette flow model of the epoxy resin system.

previous work [45], and only some essential simulation details are mentioned here. To initiate the shear flow, we superimpose a linear velocity profile on the velocity of particle i ($\mathbf{v}_0^i$) after thermoequilibration. A homogeneous shear rate ($\dot{\gamma}$) of 1E8 s^{-1} is adopted. After 1E6 time steps when the system reaches steady shear flow, the velocity profiles and the system stress tensor are collected. Time averaging of the stress tensor is performed over 500 time instances with a time interval of 1 fs.

Results and discussion

Glass transition temperature and thermal expansion coefficient

During continuous cooling, the glass transition could occur due to the failure of a system to achieve full thermodynamic equilibrium, which is a kinetic phenomenon determined by the temperature-dependent structural relaxation processes. A change in the thermal expansion coefficient, defined by $\alpha = \frac{1}{\tilde{V}}\left(\frac{\partial \tilde{V}}{\partial T}\right)_P$, where $\tilde{V}$ is the specific volume, is often used to estimate the glass transition temperatures T_g. Figure 6 shows the average specific volume of the epoxy resin system obtained at various temperatures ranging from 25 to 500 K. The densities are observed to gradually increase as the samples are steadily cooled down. The slope of the density–temperature curve can give the thermal expansion coefficient, whose noticeable decrease is an indication that glass transition is occurring. In other words, T_g is estimated from the intersection of the two linear lines that are fitting the data in the low and high temperature range, respectively, as shown in Figure 6. The estimated glass transition temperature T_g of the cured network is 360–400 K, generally in good agreement with the experimentally tested ~400 K [33]. The discrepancies could possibly be attributed to the differences between the experimental cooling rates and those adopted in our simulation.

The extracted thermal expansion coefficients and specific volume as well as their variation with cross-linking degree are listed in Tables 1 and 2, respectively. The predicted thermal expansion coefficient is within the range 1.62–2.49 E-4 K^{-1}, in fairly good agreement with the experimentally obtained value of 2.46 E-4 K^{-1}. Such volume shrinkage or increase in density has been observed experimentally during the process of network formation for epoxy-based systems. For highly dense systems (~92% cross-linking), a volume shrinkage of 5–7% was observed in our simulations. This shows good agreement with Kamorov et al. [31], Yarovsky and Evans [27], and Varshney et al. [24], where a volume shrinkage of 5–12% has been observed for different systems in these studies.

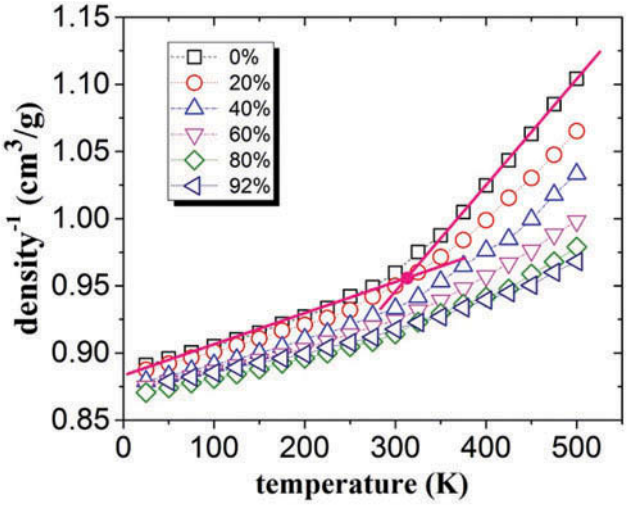

Figure 6. Variation in specific volume at various temperatures of differently cross-linked resin systems.

Table 1. Glass transition temperature T_g and thermal expansion coefficients α[a].

	0%	20%	40%	60%	80%	92%
T_g (K)	287 ± 5	295 ± 10	321 ± 10	350 ± 10	361 ± 20	380 ± 20
α_r (1E-4 K^{-1})	6.92	5.22	4.53	3.68	3.00	2.36
α_g (1E-4 K^{-1})	2.49	2.17	2.10	1.95	1.70	1.62

[a]Here α_g represents the thermal expansion coefficient at the glassy state (i.e., below the glass transition temperature) and α_r represents the thermal expansion coefficient at the rubbery state (i.e., above the glass transition temperature).

Table 2. Specific volume $\tilde{V}$ at various temperatures.

$\tilde{V}$ (cm^3/g)	0%	20%	40%	60%	80%	92%
300 K	0.960	0.950	0.933	0.924	0.914	0.918
325 K	0.975	0.960	0.942	0.931	0.923	0.922
350 K	0.988	0.972	0.953	0.939	0.929	0.927
375 K	1.005	0.984	0.964	0.948	0.936	0.934
400 K	1.025	0.999	0.976	0.957	0.941	0.939
425 K	1.044	1.016	0.984	0.966	0.948	0.945
450 K	1.063	1.030	0.999	0.976	0.959	0.950
475 K	1.085	1.047	1.017	0.988	0.967	0.960
500 K	1.104	1.065	1.033	0.998	0.978	0.968

The volume shrinkage at a certain cross-linking degree α at different temperatures $V_{s\alpha}{}^{\mathrm{T}}$ $(=1-\tilde{V}_{\alpha}^{T}/\tilde{V}_{0}^{T})$ can be computed based on Tables 2. It has been proposed that the following model can be applied to estimate the $V_{s\alpha}{}^{\mathrm{T}}$ [46]:

$$V_{S\alpha}^{T}=V_{S\infty}^{T}\cdot\alpha_{\mathrm{mod}},\alpha_{\mathrm{mod}}=\frac{\alpha-\alpha_{C1}}{\alpha_{C2}-\alpha_{C1}}, \tag{2}$$

where α_{C1}, α_{C2} represent the bounds on the degree of cure between which the resin modulus is assumed to develop, and $V_{S\infty}^{T}$ is the estimated total volumetric resin shrinkage at temperature T.

The change in volume shrinkage with different curing degrees is given in Figure 7. It can be observed the linear relation is generally obeyed at low curing degrees and the nonlinear behavior becomes obvious at 60–80% curing degree. The nonlinear behavior or, as in previous work, bilinear behavior is often ascribed to the interplay of gelation and vitrification process, which could

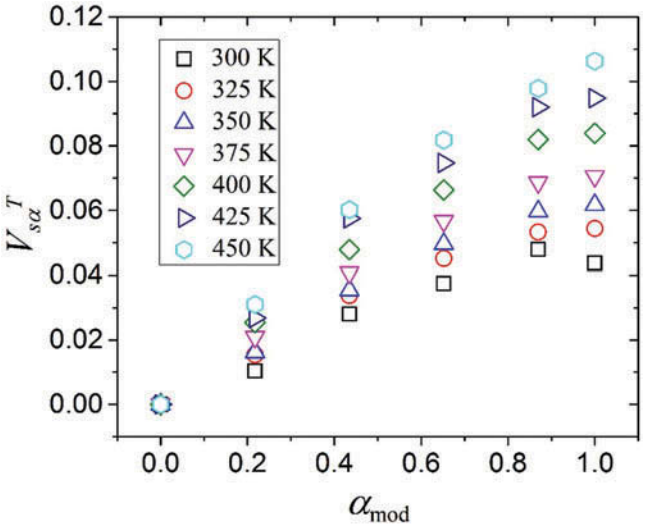

Figure 7. Volume shrinkage VsαT versus αmod at various temperatures.

determine whether the polymers are in the liquid, viscoelastic, or elastic state and the microscopic motion of polymer chains [47].

We estimated the gel point from the inflection point of the molecular weight of the largest group (Figure 8). Even though it is quite difficult to identify the inflection point with great accuracy from the few points obtained, it could be safely said that the gel point occurs between 0.6 and 0.8.

Elastic modulus and yield stress

As mentioned previously, we adopted the dynamic method [19] for the purpose of estimating the mechanical properties of epoxy systems, which has been found to achieve consistent results with experiments even when conducted at much smaller system size and higher strain rate. Either stress or strain can be controlled with the other quantity monitored during the loading process.

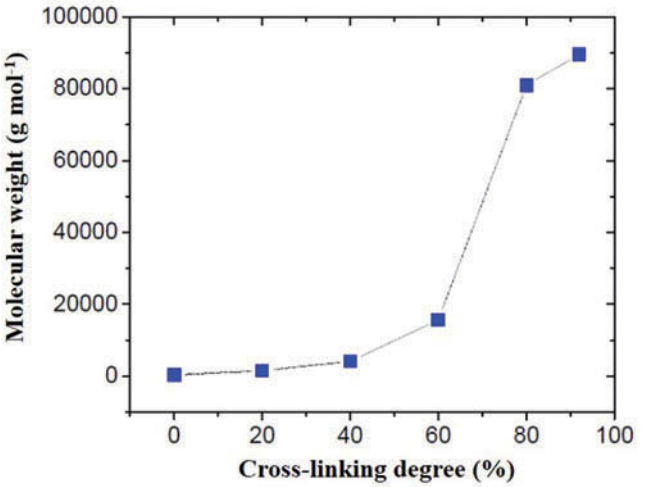

Figure 8. Molecular weight of the largest molecule as a function of the cross-linking degree.

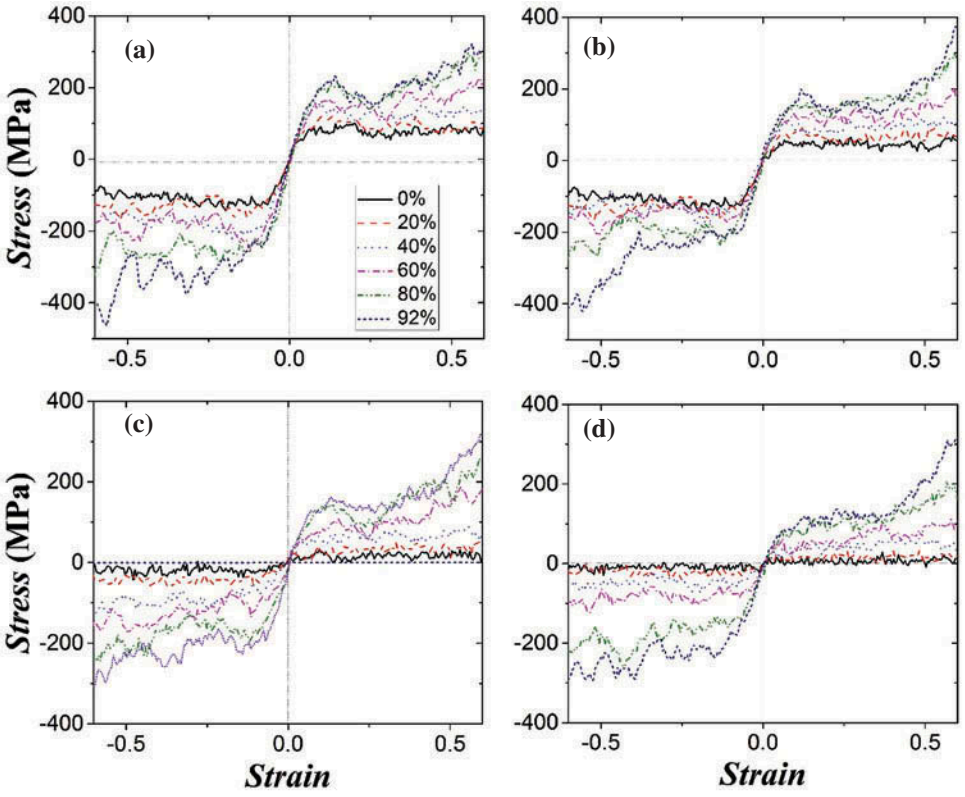

Figure 9. True stress–strain curves of the differently cross-linked systems at (a) 300 K, (b) 350 K, (c) 400 K, and (d) 450 K.

Controlling strain is favored in the current study for observing the strain softening effect. There are other computational techniques such as static and fluctuation approaches to obtain mechanical properties through molecular simulations. The static approach (or a constant-strain minimization method) is often used to obtain the entire stiffness matrix [25] for the studied material at 0 K. This method is not favored if one is interested in the elastic constants at finite temperatures. The fluctuation formula [48] is computationally expensive to perform due to the very long simulation time needed. Figure 9 shows the stress–strain curves of the differently cross-linked systems at various temperatures. The lateral stress that remains approximately zero is not shown here. The longitudinal stress shows a linear elastic regime up to approximately 8% strain. The uniaxial stress–strain curves of the systems with high cross-linking levels at 300 K demonstrate the few typical stages of a polymeric system: (1) the stress increases almost linearly related to the strain up to the point of yield in the first stage; (2) the system undergoes a slight strain softening up to a 20–30% strain in the second stage; and (3) the system experiences strain hardening or plateau in the third stage. The strain softening could be possibly attributed to the relaxation of polymer conformation and the reorientation of polymer strands for a more energetically favorable configuration in the conformational space. The hardening process may be related to the orientation of polymer strands along the loading directions, which are successively stretched resulting in increasing stress. It is worth mentioning that there are still controversies regarding the microscopic explanations of the strain softening and hardening behaviors that require further investigations. The strain softening and strain hardening behaviors become less obvious with increasing temperature and decreasing cross-linking degree, probably due to the accelerated relaxation and reorientation processes of polymer strands. The evolution of different energy contributions including bond stretching, bending, torsional, and pairwise (LJ + coulombic) interaction is shown in Figure 10. Most apparent changes can be observed

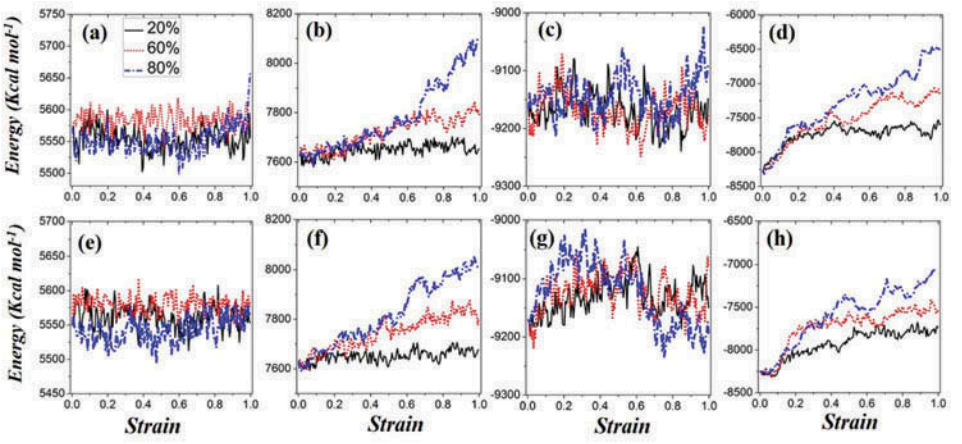

Figure 10. Evolution of different energy contributions including bond stretching, bending, torsional, and pairwise (LJ + coulombic) interaction (a)–(d) under tension and (e)–(h) under compression.

for bending and pairwise interaction, which increase with strain under both tension and compression. The magnitude of the increase also becomes larger with cross-linking degree. Bond stretching only demonstrates a small deviation from equilibrium at very high strain level and cross-linking degree. No clear tendency in energy evolution is found for torsional degree of freedom.

The Young's modulus was extracted by performing linear regression on the raw stress–strain data obtained from MD simulation with the dynamic method. The uncertainty could be caused by the choice of strain range used for the linear regression. In this work, the strain range used is $[0, \varepsilon_e]$ with ε_e varying from 5 to 8% in both the tensile and compressive regimes. The estimated modulus is thereafter used to calculate the 0.2% offset yield stress. We also plotted the lateral versus longitudinal strain relationship in Figure 11. Here the lateral strain is represented by the average of compressive/tensile strains along the y and z directions. The Poisson's ratio can then be extracted from data shown in Figure 11 by linear fitting as demonstrated in Figure 12. Following the same approach used for the Young's modulus, we found that the value of Poisson's ratio is 0.44–0.5, showing a gradual

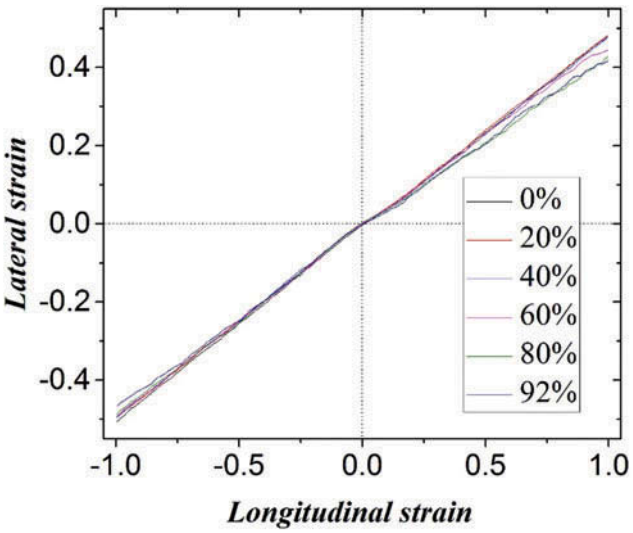

Figure 11. Lateral versus longitudinal strain curves of the differently cross-linked systems at 300 K.

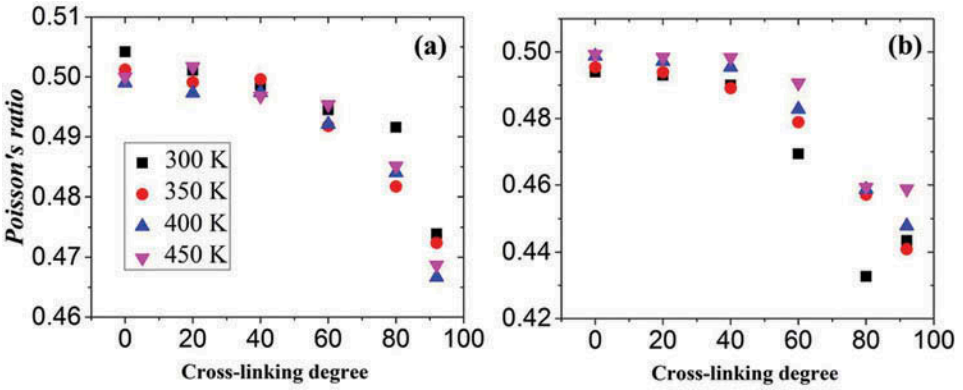

Figure 12. Poisson's ratio under compression (a) and tension (b) for the differently cross-linked systems at various temperatures.

transition from incompressible fluid to solid with increasing curing degree. The values of Poisson's ratio of 80–92% cured systems fall in the range of 0.30–0.46 for typical glassy state thermosetting polymers. No clear influence from temperature can be observed for the epoxy resins under compression, yet an increase in Poisson's ratio with temperature can be observed for those under tension.

The transition of elastic modulus around the glass transition temperature can be identified by the drastic drop between 300 and 350 K for systems of lower cross-linking degrees (0 and 20%) and between 350 and 400 K for systems of medium cross-linking degrees (40 and 60%), indicative of significant softening of the epoxy system in its rubbery state (Figure 13). For the high cross-linking

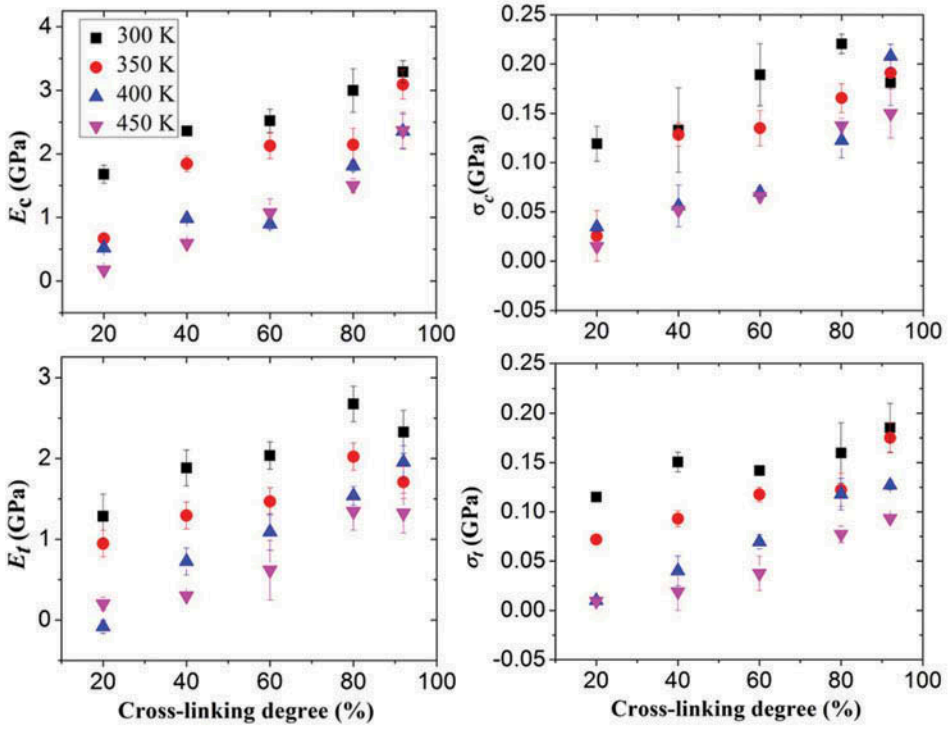

Figure 13. Extracted Young's modulus (E) and yield stress (□) under compression and tension for the differently cross-linked systems at various temperatures.

degree systems (80 and 92%), the transition is less obvious, which shows a more gradual change with smaller reduction in magnitude with temperature. Note that the glass transition temperature can also be defined by the temperature at which the elastic moduli drop significantly. The T_g estimated based on this definition is slightly higher than the one calculated previously, partly due to the high cooling rate of the cooling simulation and the high deformation rate of the dynamic simulation. It can also be observed that the Young's modulus and yield stress generally demonstrate an increasing tendency with cross-linking degree. As expected, the magnitudes of the extracted mechanical properties under compression are higher than those under tension. It has been commonly observed in both experimental and computational work that stress–strain curves of a compression test do not reproduce the tensile test because the flaws in materials more easily play a role under tension, whereas compression tests tend to be characteristic of a pure material. For example, polymer can fail in a brittle-like fashion under tension but in a ductile manner during compression [49].

The commonly used empirical model for the elastic modulus of thermoset resin with different curing degrees is be given by [7]

$$E = (1 - \alpha_{\text{mod}})E^0 + \alpha_{\text{mod}}E^\infty + \gamma\alpha_{\text{mod}}(1 - \alpha_{\text{mod}})\left(E^\infty - E^0\right), \tag{3}$$

where E^0, E^∞ are the fully uncured and fully cured temperature-dependent resin modulus, and γ is introduced to account for the competing mechanisms between stress relaxation and chemical hardening.

The above equation can be rearranged and written as a polynomial function of α_{mod}:

$$E = -\gamma\left(E^\infty - E^0\right)\alpha_{\text{mod}}^2 + (1 + \gamma)\left(E^\infty - E^0\right)\alpha_{\text{mod}} + E^0. \tag{4}$$

By fitting the elastic modulus E and α_{mod} relation (Figure 14), an estimation of the E^∞ and γ can be obtained as given in Table 3.

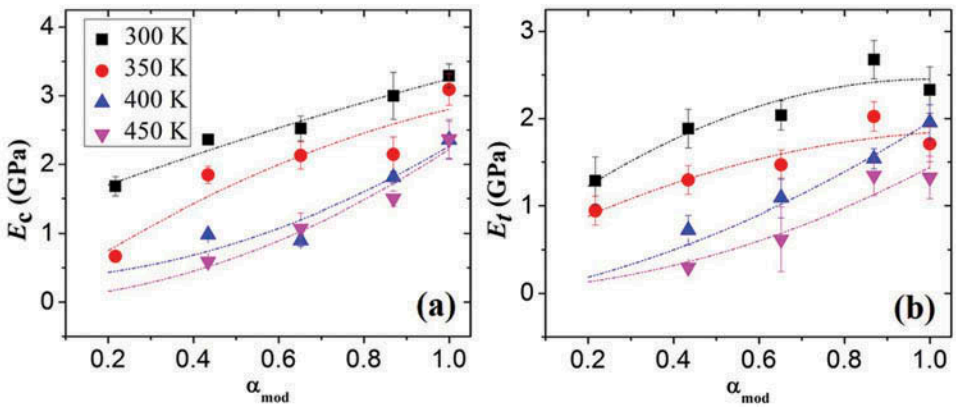

Figure 14. Elastic modulus E versus αmod under (a) compression and (b) tension at various temperatures.

Table 3. Fitted parameters for the model given in Equation (4) under compression and tension.

		300 K	350 K	400 K	450 K
Compression	E^∞ (GPa)	3.639	3.353	2.188	2.204
	γ	−0.181	−0.482	0.883	0.834
Tension	E^∞ (GPa)	2.953	2.158	2.089	1.439
	γ	−0.989	−0.770	0.546	0.820

Shearing viscosity

In the case of steady-state simple shear flows, the shear viscosity parameter η can be computed as the ratio of the steady-state shear stress $\langle \sigma_{xy}(t) \rangle$ to the shear rate $\dot{\gamma}$ [49]

$$\eta(\dot{\gamma}) = \lim_{t \to \infty} \frac{\langle \sigma_{xy}(t) \rangle}{\dot{\gamma}} = - \lim_{t \to \infty} \frac{\langle P_{xy}(t) \rangle}{\dot{\gamma}}, \tag{5}$$

where $\langle \cdot \rangle$ represents ensemble averaging. The 0% cross-linked epoxy resin follows Newtonian behavior at the chosen shear rate based on our previous experience [45], in which stage the shear stress linearly increases with shear rate. Xu et al. [50] have shown that three regions separated by two characteristic shear rates (i.e., the non-Newtonian transition shear rate $\dot{\gamma}_{nt}$ and the critical shear rate $\dot{\gamma}_{cr}$) can be found in the shear viscosity–shear rate profile. As the shear rate gradually increases, the system enters the shear-thinning (non-Newtonian) region from the constant (Newtonian) region, indicated by the non-Newtonian transition shear rate $\dot{\gamma}_{nt}$. Then it enters a third region with a further increase in shear rate, defined by the critical shear rate $\dot{\gamma}_{cr}$. Compared with the non-cross-linked melts, the non-Newtonian transition shear rate $\dot{\gamma}_{nt}$ is shifted to lower values for cross-linked ones. This effect becomes more apparent as the cross-linking degree increases. For highly cross-linked systems such as 80 and 92% cross-linked epoxy resins, the Newtonian region almost disappears and thus the viscosity computed at our chosen shear rate could be smaller than those calculated at lower shear rates. However, the quality of the data obtained at very low shear rates is very poor, due to the large thermal noises that can create a high noise-to-signal ratio, which can only be reduced by a large temporal averaging window size. Thus, we did not choose very low shear rates, which leads to prohibitively long simulation time to provide a reasonably accurate prediction.

Another commonly used approach to compute the Newtonian shear viscosity is the Green-Kubo formulation after a step shear deformation is applied [51]

$$\eta = \int_0^\infty G(t) \mathrm{d}t, \tag{6}$$

where the time-dependent shear modulus $G(t)$ is computed from the stress autocorrelation function (SACF) given by

$$G(t) = \frac{V}{k_B T} \langle \sigma_{\alpha\beta}(t) \sigma_{\alpha\beta}(0) \rangle, \tag{7}$$

where V is the system volume, T is the temperature, and the stress component $\sigma_{\alpha\beta}$ can be calculated via the virial theorem

$$\sigma_{\alpha\beta} = \frac{1}{V} \left(\sum\nolimits_{i=1}^{n} m_i v_{i\alpha} v_{i\beta} + \frac{1}{2} \sum_{\substack{i,j=1 \\ i \neq j}}^{n} r_{ij\alpha} f_{ij\beta} \right). \tag{8}$$

Here m_i, $v_{i\alpha}$, and $v_{i\beta}$ are the mass and the α- and β-component velocities of atom i, respectively; and $r_{ij\alpha}$ and $f_{ij\beta}$ are the α-component relative postion and β-component force acting between atoms i and j, respectively. In our future work, we would like to compare the computed viscosity from these two different approaches.

The rheological behavior of thermoset resins is governed by two main physical mechanisms as revealed by Figure 15. On the one hand, the viscosity decreases with temperature as a result of the higher mobility of the polymer chains. On the other hand, the cross-linking reactions, which are thermally activated, lead to an increase in viscosity. The resin viscosity has been assumed to be influenced by the temperature T and curing degree α in an uncoupled manner in the proposed empirical equations [52]

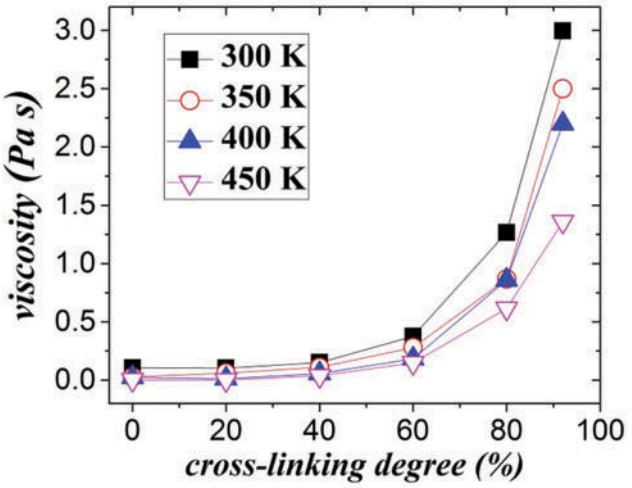

Figure 15. Variation in viscosity with cross-linking degree at different temperatures.

$$\eta(T,\alpha) = A_\eta \exp\left(K_\mu \alpha\right) \tag{9a}$$

$$A_\eta = \eta_\infty \exp\left(-\frac{E_\eta}{RT}\right), \tag{9b}$$

where R is the gas constant, and the constants η_∞, K_μ, and E_η are determined by fitting to the simulation data, given in Table 4. This proposed model with fitted parameters can agree fairly well with the simulation data in Figure 15; however, larger discrepancies can still be found at lower cross-linking degrees.

Conclusions

In this article, MD simulations are conducted to estimate the thermomechanical properties of a widely used epoxy resin system consisting of DGEBA resin and and IPD cross-linker. A multistep cross-linking and relaxation procedure is adopted to construct the simulation cell of differently cross-linked systems, which allows for creating a high cross-linking degree from a given set of monomers. The ab initio PCFF is used to describe the interatomic interactions during the MD simulations. The thermomechanical properties including glass transition temperature, thermal expansion coefficient, curing-induced shrinkage, Young's modulus, Poisson's ratio, yield strength, and viscosity, which are critically important to the formation of manufacturing defects during the autoclave process, are estimated. The dependence of these properties on the cross-linking degree and temperature that vary during the autoclave process is also identified and analyzed via empirical continuum models.

It has been shown that in most cases, MD simulations produce predictions similar to those reported by experimental methods. Some factors that may influence the prediction from MD techniques include failing to consider the long-range forces in polymers that exceed the size of the simulation cell and extremely high cooling rate and strain rate used in MD. Though the latter factor is also faced by crystalline materials, it is much more severe for polymers due to its viscoelastic and plastic nature.

Table 4. Fitted parameters for the model given in Equations (9a) and (9b).

η_∞	K_μ	E_η
4.78E-5	0.0641	−1.44E4

Funding

This work utilized the Janus supercomputer, which is supported by the National Science Foundation (award number CNS-0821794) and the University of Colorado Boulder. The Janus supercomputer is a joint effort of the University of Colorado Boulder, the University of Colorado Denver, and the National Center for Atmospheric Research. The second author acknowledges support by the Office of Naval Research through the core funding by the Naval Research Laboratory.

References

1. M. Gupta and R. Srivastava, Mechanical Properties of Hybrid Fibers-Reinforced Polymer Composite: A Review, *Polymer-Plastics Technology and Engineering*, Vol. 55, No. 6, pp. 626–642, 2016.
2. J.G. Michopoulos, S.G. Lambrakos, and A. Iliopoulos, On a Data and Requirements Driven Multi-Scale Framework Linking Performance to Materials, *ASME* 2010 *International Design Engineering Technical Conferences and Computers and Information in Engineering Conference*, Montreal, QC, Canada, 15–18 August, 2010.
3. J. Wang, K. Potter, and J. Etches, Experimental Investigation and Characterisation Techniques of Compressive Fatigue Failure of Composites with Fibre Waviness at Ply Drops, *Composite Structures*, Vol. 100, pp. 398–403, 2013.
4. Y. Ledru, R. Piquet, F. Schmidt, L. Michel, and G. Bernhart, Modeling of Voids Growth Mechanisms during Manufacturing Composites Laminates, *9th International Conference on Flow Processes in Composite Materials—FPCM-9*, Montréal, QC, Canada, 7–9 July, 2008.
5. T. Mesogitis, A. Skordos, and A. Long, Uncertainty in the Manufacturing of Fibrous Thermosetting Composites: A Review, *Composites Part A: Applied Science and Manufacturing*, Vol. 57, pp. 67–75, 2014.
6. V. Kaushik and J. Raghavan, Experimental Study of Tool–Part Interaction during Autoclave Processing of Thermoset Polymer Composite Structures, *Composites Part A: Applied Science and Manufacturing*, Vol. 41, pp. 1210–1218, 2010.
7. G. Abdelal, A. Robotham, and W. Cantwell, Autoclave Cure Simulation of Composite Structures Applying Implicit and Explicit FE Techniques, *International Journal of Mechanics and Materials in Design*, Vol. 9, pp. 55–63, 2012.
8. Y. Gu, M. Li, Z. Zhang, and Y. Li, Effects of Resin Storage Aging on Rheological Property and Consolidation of Composite Laminates, *Polymer Composites*, Vol. 30, pp. 1081–1090, 2009.
9. X. Yan, Finite Element Modeling of Curing of Epoxy Matrix Composites, *Journal of Applied Polymer Science*, Vol. 103, pp. 2310–2319, 2007.
10. O. Kravchenko, C. Li, A. Strachan, S. Kravchenko, and R. Pipes, Prediction of the Chemical and Thermal Shrinkage in a Thermoset Polymer, *Composites Part A: Applied Science and Manufacturing*, Vol. 66, pp. 35–43, 2014.
11. Y. Li, M. Li, Y. Gu, and Z. Zhang, Numerical and Experimental Study on the Effect of Lay-Up Type and Structural Elements on Thickness Uniformity of L-Shaped Laminates, *Applied Composite Materials*, Vol. 16, pp. 101–115, 2009.
12. S. Advani and E. Sozer, *Process Modeling in Composites Manufacturing*, 2nd ed., CRC Press, Boca Raton, FL, 2010.
13. Y. Fu and J.-H. Song, On Computing Stress in Polymer Systems Involving Multi-Body Potentials from Molecular Dynamics Simulation, *Journal of Chemical Physics, 141*(5), p. 054108, 2014.
14. Y. Fu and J.-H. Song, Heat Flux Expressions That Satisfy the Conservation Laws in Atomistic System Involving Multibody Potentials, *Journal of Computational Physics*, 294 pp. 191–207, 2015.
15. M. Stevens, Manipulating Connectivity to Control Fracture in Network Polymer Adhesives, *Macromolecules*, Vol. 34, pp. 1411–1415, 2001.
16. M. Tsige and M. Stevens, Effect of Cross-Linker Functionality on the Adhesion of Highly Cross-Linked Polymer Networks: A Molecular Dynamics Study of Epoxies, *Macromolecules*, Vol. 37, pp. 630–637, 2004.
17. I. Carmesin and K. Kremer, The Bond Fluctuation Method: A New Effective Algorithm for the Dynamics of Polymers in All Spatial Dimensions, *Macromolecules*, Vol. 21, pp. 2819–2823, 1988.
18. W. Jo and M. Ko, Effect of Reactivity on Cure and Phase Separation Behavior in Epoxy Resin Modified with Thermoplastic Polymer: A Monte Carlo Simulation Approach, *Macromolecules*, Vol. 27, pp. 7815–7824, 1994.
19. Y. Fu and J.-H. Song, Large Deformation Mechanism of Glassy Polyethylene Polymer Nanocomposites: Coarse Grain Molecular Dynamics Study, *Computational Materials Science*, Vol. 96, pp. 485–494, 2015.
20. Y. Fu, J. Michopoulos, and J.-H. Song, Dynamics Response of Polyethylene Polymer Nanocomposites to Shock Wave Loading, *Journal of Polymer Science, Part B: Polymer Physics*, Vol. 53, pp. 1292–1302, 2015.
21. M. Grujicic, B. Pandurangan, W. Bell, B. Cheeseman, C. Yen, and C. Randow, Molecular-Level Simulations of Shock Generation and Propagation in Polyurea, *Materials Science and Engineering: A*, Vol. 528, pp. 3799–3808, 2011.

22. A. Bandyopadhyay, P. Valavala, T. Clancy, K. Wise, and G. Odegard, Molecular Modeling of Crosslinked Epoxy Polymers: The Effect of Crosslink Density on Thermomechanical Properties, *Polymer*, Vol. 52, pp. 2445–2452, 2011.
23. C. Li and A. Strachan, Molecular Dynamics Predictions of Thermal and Mechanical Properties of Thermoset Polymer EPON862/DETDA, *Polymer*, Vol. 52, pp. 2920–2928, 2011.
24. V. Varshney, S. Patnaik, A. Roy, and B. Farmer, A Molecular Dynamics Study of Epoxy-Based Networks: Cross-Linking Procedure and Prediction of Molecular and Material Properties, *Macromolecules*, Vol. 41, pp. 6837–6842, 2008.
25. C. Wu and W. Xu, Atomistic Molecular Modelling of Crosslinked Epoxy Resin, *Polymer*, Vol. 47, pp. 6004–6009, 2006.
26. S. Yang and J. Qu, Computing Thermomechanical Properties of Crosslinked Epoxy by Molecular Dynamic Simulations, *Polymer*, Vol. 53, pp. 4806–4817, 2012.
27. I. Yarovsky and E. Evans, Computer Simulation of Structure and Properties of Crosslinked Polymers: Application to Epoxy Resins, *Polymer*, Vol. 43, pp. 963–969, 2002.
28. J. Gou, B. Minaie, B. Wang, Z. Liang, and C. Zhang, Computational and Experimental Study of Interfacial Bonding of Single-Walled Nanotube Reinforced Composites, *Computational Materials Science*, Vol. 31, pp. 225–236, 2004.
29. H. Fan and M. Yuen, Material Properties of the Cross-Linked Epoxy Resin Compound Predicted by Molecular Dynamics Simulation, *Polymer*, Vol. 48, pp. 2174–2178, 2007.
30. C. Wu and W. Xu, Atomistic Simulation Study of Absorbed Water Influence on Structure and Properties of Crosslinked Epoxy Resin, *Polymer*, Vol. 48, pp. 5440–5448, 2007.
31. P. Komarov, C. Yu-Tsung, C. Shih-Ming, P. Khalatur, and P. Reineker, Highly Cross-Linked Epoxy Resins: An Atomistic Molecular Dynamics Simulation Combined with a Mapping/Reverse Mapping Procedure, *Macromolecules*, Vol. 40, pp. 8104–8113, 2007.
32. Material Studio, Accelrys Inc./Biovia. Available at: http://accelrys.com/products/collaborativescience/. (Accessed 19 June–19 July 2015)
33. O. Sindt, J. Perez, and J. Gerard, Molecular Architecture—Mechanical Behaviour Relationships in Epoxy Networks, *Polymer*, Vol. 37, pp. 2989–2997, 1996.
34. H. Sun, Force Field for Computation of Conformational Energies, Structures, and Vibrational Frequencies of Aromatic Polyesters, *Journal Computational Chemistry*, Vol. 15, pp. 752–768, 1994.
35. H. Sun, S. Mumby, J. Maple, and A. Hagler, An ab Initio CFF93 All-Atom Force Field for Polycarbonates, *Journal of the American Chemical Society*, Vol. 116, pp. 2978–2987, 1994.
36. J. Maple, U. Dinur, and A. Hagler, Derivation of Force Fields for Molecular Mechanics and Dynamics from ab initio Energy Surfaces, *Proceedings of the National Academy of Sciences*, Vol. 85, pp. 5350–5354, 1988.
37. M. Hwang, T. Stockfisch, and A. Hagler, Derivation of Class II Force Fields. 2. Derivation and Characterization of a Class II Force Field, CFF93, for the Alkyl Functional Group and Alkane Molecules, *Journal of the American Chemical Society*, Vol. 116, pp. 2515–2525, 1994.
38. J.R. Maple, U. Dinur, and A.T. Hagler, Derivation of Force Fields for Molecular Mechanics and Dynamics from ab initio Energy Surfaces, *PNAS, Proceedings of the National Academy of Sciences*, pp. 5350–5354, 1988.
39. J.R. Maple, M.-J. Hwang, T.P. Stockfisch, U. Dinur, M. Waldman, C.S. Ewig, and A.T. Hagler, Derivation of Class II Force Fields. I. Methodology and Quantum Force Field for the Alkyl Functional Group and Alkane Molecules, *Journal of Computational Chemistry*, Vol. 15, p. 162–182, 1994.
40. S. Plimpton, Fast Parallel Algorithms for Short-Range Molecular Dynamics, *Journal of Computational Physics*, Vol. 117, pp. 1–19, 1995.
41. S. Nosé, A Unified Formulation of the Constant Temperature Molecular Dynamics Methods, *The Journal of Chemical Physics*, Vol. 81, pp. 511–519, 1984.
42. W. Hoover, Canonical Dynamics: Equilibrium Phase-Space Distributions, *Physical Review A*, Vol. 31, pp. 1695–1697, 1985.
43. P. Padilla and S. Toxvaerd, Simulating Shear Flow, *The Journal of Chemical Physics*, Vol. 104, pp. 5956–5963, 1996.
44. H. Kobayashi and R. Yamamoto, Implementation of Lees–Edwards Periodic Boundary Conditions for Direct Numerical Simulations of Particle Dispersions under Shear Flow, *The Journal of Chemical Physics*, Vol. 134, p. 064110, 2011.
45. Y. Fu, J. Michopoulos, and J.-H. Song, Coarse-Grained Molecular Dynamics Simulations of Epoxy Resin during the Curing Process, *Computational Materials Science*, Vol. 107, pp. 24–32, 2015.
46. T. Bogetti and J. Gillespie, Process-Induced Stress and Deformation in Thick-Section Thermoset Composite Laminates, *Journal of Composite Materials*, Vol. 26, pp. 626–660, 1992.
47. L. Khoun and P. Hubert, Cure Shrinkage Characterization of an Epoxy Resin System by Two in Situ Measurement Method, *Polymer Composites*, Vol. 31, No. 9, pp. 1603–1610, 2010.
48. A.A. Gusev, M.M. Zehnder, and U.W. Suter, Fluctuation Formula for Elastic Constants, *Physical Review B*, Vol. 54, pp. 1–4, 1996.

49. X. Yong and L. Zhang, Nanoscale Simple-Fluid Behavior under Steady Shear, *Physical Review E*, Vol. 85, p. 051202, 2012.
50. X. Xu, J. Chen, and L. An, Shear Thinning Behavior of Linear Polymer Melts under Shear Flow via Nonequilibrium Molecular Dynamics, *The Journal of Chemical Physics*, Vol. 140, p. 174902, 2014.
51. B. Arman, A. Reddy, and G. Arya, Viscoelastic Properties and Shock Response of Coarse-Grained Models of Multiblock versus Diblock Copolymers: Insights into Dissipative Properties of Polyurea, *Macromolecules*, Vol. 45, pp. 3247–3255, 2012.
52. W.I. Lee, A. Loos, and G. Springer, Heat of Reaction, Degree of Cure, and Viscosity of Hercules 3501-6 Resin, *Journal of Composite Materials*, Vol. 16, pp. 510–520, 1982.